Biochemistry

Article

pubs.acs.org/biochemistry

# Conformational Control of UDP-Galactopyranose Mutase Inhibition

Kittikhun Wangkanont,[†,∥] Valerie J. Winton,[†] Katrina T. Forest,[*,†,§] and Laura L. Kiessling[*,†,‡]

[†]Department of Chemistry, [‡]Department of Biochemistry, and [§]Department of Bacteriology, University of Wisconsin—Madison, Madison, Wisconsin 53706, United States

Supporting Information

**ABSTRACT:** UDP-galactopyranose mutase (Glf or UGM) catalyzes the formation of uridine 5′-diphosphate-α-D-galactofuranose (UDP-Gal*f*) from UDP-galactopyranose (UDP-Gal*p*). The enzyme is required for the production of Gal*f*-containing glycans. UGM is absent in mammals, but members of the Corynebacterineae suborder require UGM for cell envelope biosynthesis. The need for UGM in some pathogens has prompted the search for inhibitors that could serve as antibiotic leads. Optimizing inhibitor potency, however, has been challenging. The UGM from *Klebsiella pneumoniae* (KpUGM), which is not required for viability, is more effectively impeded by small-molecule inhibitors than are essential UGMs from species such as *Mycobacterium tuberculosis* or *Corynebacterium diphtheriae*. Why KpUGM is more susceptible to inhibition than other orthologs is not clear. One potential source of difference is UGM ortholog conformation. We previously determined a structure of CdUGM bound to a triazolothiadiazine inhibitor in the open form, but it was unclear whether the small-molecule inhibitor bound this form or to the closed form. By varying the terminal tag (CdUGM-His$_6$ and GSG-CdUGM), we crystallized CdUGM to capture the enzyme in different conformations. These structures reveal a pocket in the active site that can be exploited to augment inhibitor affinity. Moreover, they suggest the inhibitor binds the open form of most prokaryotic UGMs but can bind the closed form of KpUGM. This model and the structures suggest strategies for optimizing inhibitor potency by exploiting UGM conformational flexibility.

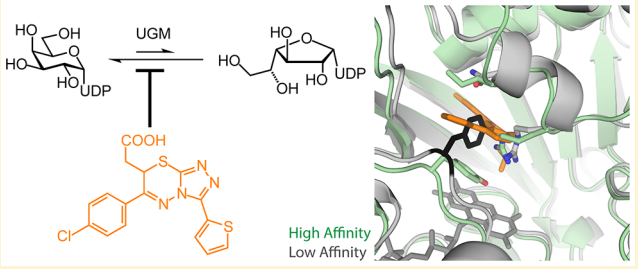


UDP-galactopyranose mutase (UGM) catalyzes the interconversion of UDP-galactopyranose (UDP-Gal*p*) and UDP-galactofuranose (UDP-Gal*f*) (Figure 1).[1−3] The latter serves as an activated sugar donor used by glycosyltransferases to synthesize Gal*f* glycoconjugates. Gal*f* residues are critical components of the galactomannan component of the *Aspergillus* cell wall[4] and the essential galactan layer of the mycobacterial and corynebacterial cell walls.[5,6] Additionally, virulence factors of *Leishmania* contain Gal*f* residues.[7,8] Although Gal*f*-containing glycans in nematodes have yet to be identified, nematodes encode a UGM, and *Caenorhabditis elegans* expresses a functional UGM.[9−11] In contrast, Gal*f* residues are not found in mammals, and mammals do not possess UGM.[12] In many organisms that encode a UGM, deletion or downregulation of UGM production has deleterious consequences,[9,13] including lethality in mycobacteria.[5,6] Accordingly, UGM inhibitors block the growth of *Mycobacterium* and *Corynebacterium* species.[14−17] These data suggest UGM is an attractive antimicrobial target, especially in *Mycobacterium tuberculosis* and drug-resistant *Corynebacterium diphtheriae*.[18]

Effective UGM inhibitors can probe the role of UGM in different organisms[17] and serve as potential antimicrobial leads. Many known inhibitors are UDP-Gal*f* analogues that bind UGM *in vitro* but have not been shown to function in cells.[19−26] Our group identified nonsubstrate analogue 2-aminothiazoles as some of the most potent UGM inhibitors described to date[14] (Figure 1). These compounds, however, exhibited some toxicity to mammalian cells and were difficult to optimize.[15,27] Through virtual screening, we found a family of triazolothiadiazine inhibitors (Figure 1) that possess improved physical properties and that are active against *M. tuberculosis*.[15] We sought to optimize these inhibitors further by understanding the molecular basis of their affinity for UGM.

We used X-ray crystallography to determine the structure of a triazolothiadiazine inhibitor bound to *C. diphtheriae* UGM (CdUGM).[15] The complex adopted an open conformation and not the closed form observed for substrate-bound *Klebsiella pneumoniae* UGM (KpUGM)[28] used in the virtual screen. The triazolothiadiazine inhibitor was bound in the active site but not in the orientation of the lowest-energy pose in the closed complex. We detected unmodeled electron density peaks under the opened lid, which might represent alternate conformation(s), in which the lid is closed over the active site. Refined occupancies of 0.81 and 0.87 for the inhibitor in each active site of the biological dimer suggest, however, that the closed conformation may be of the unliganded state. These data suggest that the UGM−inhibitor complexes can adopt multiple conformations and create uncertainty about the preferred inhibitor binding modes.[15] Given that inhibitor affinity differs among UGM orthologs, we sought to analyze variations in

**Received:** March 2, 2017
**Revised:** June 6, 2017
**Published:** June 13, 2017




DOI: 10.1021/acs.biochem.7b00189
*Biochemistry* 2017, 56, 3983−3992

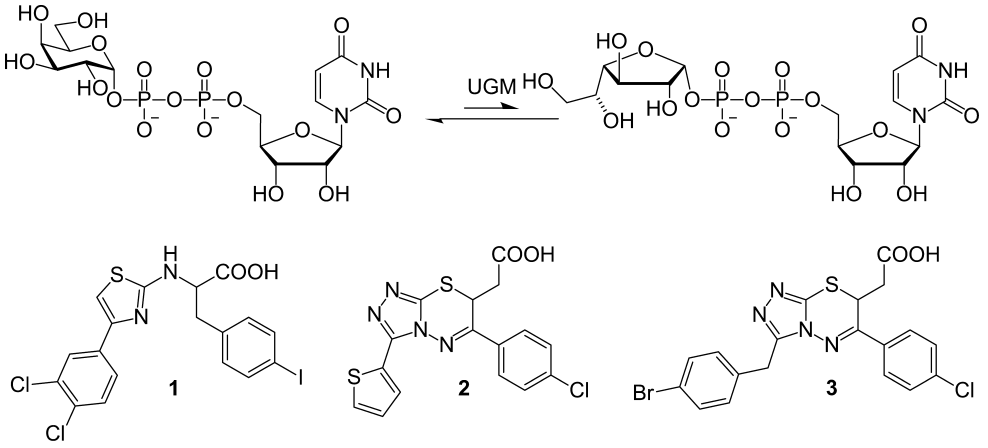


**Figure 1.** UGM catalyzes the interconversion of UDP-Gal*p* and UDP-Gal*f*, and the enzyme can be inhibited by 2-aminothiazoles, such as **1**, or triazolothiadiazines, such as **2** and **3**.

UGM conformation and extrapolate their consequences for inhibitor binding.

All of the small-molecule, heterocyclic UGM inhibitors studied to date are more potent against KpUGM than against other UGM orthologs that have been tested.[14,15] For example, the $K_i$ value of the triazolothiadiazine inhibitor against KpUGM is 8 ± 3 $\mu$M, a value ~4-fold better than that for *M. tuberculosis* (MtUGM) (31 ± 18 $\mu$M) and 10-fold better than that for CdUGM (77 ± 37 $\mu$M). Other analogues show larger differences, as illustrated by the different $K_i$ values for compound **3** (Figure 1) for KpUGM (1.1 ± 0.2 $\mu$M) and CdUGM (29 ± 8 $\mu$M).[15] Indeed, superior inhibitory activity against KpUGM is observed for the triazolothiadiazine inhibitors as well as the 2-aminothiazole inhibitors tested.[14,15] The active sites of the orthologous enzymes are similar. Neither sequence variation nor structural studies to date reveal a molecular basis for the affinity differences. Understanding these differences, however, could guide the development of more potent inhibitors that serve as leads for pulmonary diseases caused by nontuberculous mycobacteria and tuberculosis. Attempts to crystallize KpUGM with inhibitors yielded crystals exhibiting lattice-translocation disorder coupled with translational pseudosymmetry[29] (unpublished results). Neither the conformation of the mobile lid in KpUGM nor the inhibitor occupancy could be determined. The challenges that arose in obtaining a structure of KpUGM bound to an inhibitor led us to re-examine the structure of CdUGM. We had obtained a structure of a complex with this ortholog, and we reasoned that using X-ray crystallography to capture CdUGM conformational features might illuminate differences between CdUGM and KpUGM.

UGM orthologs are conformationally dynamic. Both prokaryotic and eukaryotic UGMs possess a mobile lid that can close over the active site.[26,28,30] In the open form, the lid lacks secondary structure and is located away from the active site. In the closed conformation, the lid adopts a helical conformation that positions a conserved arginine to interact with the substrate UDP-Gal*p*.[31] Comparison of oxidized and reduced KpUGM structures showed reduction *in crystallo* accompanied by a move in the mobile lid toward the substrate.[28] Minor variations in lid conformation have also been reported in the structures of other prokaryotic UGMs. Though the position of the conserved arginine in KpUGM[28] suggests the residue mainly interacts with the pyrophosphoryl group of the UDP-Gal*p* substrate, in the *Deinococcus radiodurans* (Dr) UGM, the corresponding arginine interacts with the pyrophosphoryl group and the galactopyranose residue.[30] Studies of the *M. tuberculosis* UGM with a nonsubstrate inhibitor suggest there is an allosteric binding pocket near the active site and that occupation of this pocket prevents loop closure.[32] Eukaryotic UGMs also adopt multiple conformations, and they have a second mobile flap containing an asparagine residue involved in substrate recognition.[33,34] Additionally, molecular dynamics studies indicate a third mobile loop near the active site in the *Trypanosoma cruzi* UGM (TcUGM).[34] Dramatic conformational changes are also observed in a histidine-containing loop in eukaryotic UGMs.[33,34] These observations highlight the flexibility of UGMs and suggest that progress in understanding UGM conformational variation would advance inhibitor design.

To determine structures of CdUGM in distinct conformations, we sought to crystallize the enzyme in multiple crystal forms. Because residues at protein termini tend to participate in crystal packing and impose alternative structural restraints, they can dramatically affect crystallization.[35] We hypothesized that by varying the tag we could obtain different crystal forms of CdUGM and thereby gain insight into the accessible conformational states of the enzyme. We therefore produced CdUGM variants with a hexahistidine tag at the C-terminus (CdUGM-$His_6$) or a three-amino acid peptide linker at the N-terminus (GSG-CdUGM). Crystallization of these fusion proteins afforded two new crystal forms of CdUGM. The resulting structures shed light on the conformational dynamics of UGM and provide new information for guiding inhibitor development.

## MATERIALS AND METHODS

**CdUGM-$His_6$ Complexed to Sodium Citrate.** The sequence encoding residues 1−387 of CdUGM was amplified using primers 5′-CGAGCAATTGACCAACAAGGACCATAGATTATGTCTGACTTTGATCTGATCGTGGTAGGT-3′ and 5′-ATTCGAGCTCTCATTAATGGTGATGGTGGTGATGTTTCAGGGCGTCGACAAGCTTGTTAT-3′. The polymerase chain reaction product was then digested and cloned into the MfeI and SalI sites of pMALc5x. The resulting construct encoded CdUGM with a C-terminal $His_6$ tag with no linker (CdUGM-$His_6$). CdUGM-$His_6$ was produced and purified using previously reported protocols.[15,36] Protein was



DOI: 10.1021/acs.biochem.7b00189
*Biochemistry* 2017, 56, 3983−3992

**Table 1. Data Collection and Refinement Statistics**

| Data collection statistics | CdUGM-$His_6$–sodium citrate complex | CdUGM-$His_6$ soaked in potassium citrate buffer | GSG-CdUGM–UDP complex |
|---|---|---|---|
| wavelength (Å) | 0.97872 | 1.18080 | 0.97856 |
| resolution range (Å)[a] | 46.72–1.95 (2.02–1.95) | 49.01–2.35 (2.43–2.35) | 29.1–2.15 (2.23–2.15) |
| space group | $P4_12_12$ | $P4_12_12$ | $C2$ |
| unit cell dimensions | 98.3, 98.3, 126.2 | 98.0, 98.0, 126.3 | 115.6, 82.7, 108.6, 90, 112.6, 90 |
| total no. of reflections | 1075063 (89525) | 378033 (33333) | 376968 (26894) |
| no. of unique reflections | 45492 (4454) | 26343 (2584) | 50316 (4637) |
| multiplicity | 23.6 (20.1) | 14.4 (12.9) | 7.5 (5.8) |
| completeness (%) | 99.9 (99.6) | 100.0 (100.0) | 97.5 (90.5) |
| mean $I/\sigma(I)$ | 36.3 (3.6) | 24.0 (3.0) | 27.4 (2.8) |
| Wilson $B$ factor (Å$^2$) | 29.3 | 37.0 | 41.9 |
| $R_{merge}$ | 0.103 (0.756) | 0.127 (0.971) | 0.064 (0.419) |
| $R_{meas}$ | 0.105 (0.775) | 0.123 (>1) | 0.069 (0.458) |
| $R_{pim}$ | 0.020 (0.164) | 0.035 (0.280) | 0.025 (0.181) |
| highest-shell $CC_{1/2}$ | (0.923) | (0.801) | (0.956) |
| **Refinement statistics** | | | |
| resolution range (Å)[a] | 46.73–1.95 (2.02–1.95) | | 28.25–2.15 (2.22–2.15) |
| $R$ factor | 0.1528 (0.1982) | | 0.1765 (0.2485) |
| $R_{free}$ (10%) | 0.1895 (0.2267) | | 0.2281 (0.3009) |
| no. of atoms | | | |
| protein | 3302 | | 6344 |
| FAD | 53 | | 106 |
| UDP | – | | 50 |
| citrate | 13 | | – |
| $Na^+$ | 2 | | – |
| water | 458 | | 228 |
| no. of protein residues | 386 | | 771 |
| RMSD for bonds (Å) | 0.008 | | 0.008 |
| RMSD for angles (deg) | 1.05 | | 1.192 |
| estimated coordinate error (ML, Å) | 0.17 | | 0.25 |
| Ramachandran favored (%) | 98.8 | | 98.4 |
| Ramachandran outliers (%) | 0 | | 0 |
| average isotropic $B$ factor (Å$^2$) | | | |
| chain A | | | |
| protein | 31.6 | | 48.1 |
| FAD | 26.5 | | 52.1 |
| UDP | – | | 37.4 |
| citrate | 32.3 | | – |
| $Na^+$ | 30.2 | | – |
| water | 41.2 | | 49.6 |
| chain B | | | |
| protein | – | | 69.6 |
| FAD | – | | 85.3 |
| UDP | – | | 56.8 |
| water | – | | 51.7 |

[a]Statistics for the highest-resolution shell are given in parentheses.

dialyzed against 20 mM Tris (pH 7.0) and concentrated to 10 mg/mL. The 2-aminothiazole inhibitor[14] was added to a final concentration of 1 mM (from a 40 mM stock in isopropanol). This inhibitor has a $K_i$ for CdUGM of 4.9 ± 1.5 μM, as determined using a previously reported HPLC-based assay.[37] Crystals were grown by hanging drop vapor diffusion using 2 μL of a protein solution and 2 μL of the well solution [100 mM sodium citrate (pH 5.6), 15% isopropanol, and 16–18% PEG 5000 MME], reaching maximal size within 3–4 days. Crystals were cryoprotected by being briefly soaked in the well solution containing 1 mM 2-aminothiazole and 20% ethylene glycol before vitrification and storage in liquid nitrogen. Single-crystal X-ray diffraction data were collected at beamline 21-ID-F (LS-CAT) at Argonne National Laboratory using a MAR225 CCD detector and processed using HKL2000.[38] Molecular replacement was performed with Phaser[39] using a previously reported KpUGM monomer structure in an open conformation [Protein Data Bank (PDB) entry 2BI7].[40] Restraints for small-molecule ligands were generated using eLBOW.[41] Model adjustment and refinement were performed with Coot and phenix.refine, respectively.[42,43] The model was validated using MolProbity.[44] Structure figures were generated with PyMOL (version 1.7, Schrödinger LLC). Data collection and refinement statistics are listed in Table 1. During refinement, the $Na^+$–O bond length was restrained to 2.43 Å with a tolerance of 0.25 Å.

To determine the sodium ion identity, crystals were grown as described above, briefly washed, and soaked for 24 h in 100 mM potassium citrate (pH 5.6), 15% isopropanol, and 18%



DOI: 10.1021/acs.biochem.7b00189
Biochemistry 2017, 56, 3983–3992

PEG 5000 MME without the 2-aminothiazole inhibitor. Cryoprotection was performed as described above, with potassium citrate replacing sodium citrate. Single-crystal X-ray diffraction data were collected at beamline 14-1 at Stanford Synchrotron Radiation Lightsource using a MAR325 CCD detector (Table 1). These data were analyzed using difference Fourier techniques; no refinement was performed.

The coordinates and structure factors for CdUGM-$His_6$ in complex with sodium citrate have been deposited in the Protein Data Bank as entry 5BR7. Structure factors for the potassium citrate-soaked crystal of CdUGM-$His_6$ were appended as the second data set under the same accession code.

**GSG-CdUGM Complexed to UDP.** Site-directed mutagenesis was performed on a previously reported CdUGM construct (G-CdUGM)[15] to add a short linker (SerGly) after the glycine of the tobacco etch virus (TEV) cleavage site for more efficient cleavage (GSG-CdUGM). The following primers were used: 5′-AGCGAAAACCTGTATTTTCAGGGTAGCG-GCATGTCTGACTTTGATCTGATCGTGGTAG-3′ and 5′-CTACCACGATCAGATCAAAGTCAGACATGCCGCTAC-CCTGAAAATACAGGTTTTCGCT-3′. GSG-CdUGM was purified using previously reported protocols.[15,36] Protein was dialyzed against 20 mM Tris (pH 7.0) and concentrated to 10 mg/mL. UDP-Gal*p* was added to a final concentration of 10 mM (from a 100 mM stock in water). Crystals were grown by hanging drop vapor diffusion using 2 $\mu$L of a protein solution and 2 $\mu$L of the well solution [100 mM Bis-Tris (pH 5.5), 200 mM lithium sulfate, and 21% PEG 3350] and reached maximal size in 1−2 weeks. Cryoprotection was achieved with a brief soak in the well solution with PEG 3350 at a final concentration of 35%. Crystals were then vitrified and stored in liquid nitrogen. Single-crystal X-ray diffraction data were collected at beamline 21-ID-G (LS-CAT) at Argonne National Laboratory using a MAR300 CCD detector. Data processing, phasing, and refinement were performed using the procedures and programs described for CdUGM-$His_6$. Molecular replacement was performed using a structure of *Mycobacterium smegmatis* UGM (MsUGM) in a closed conformation (PDB entry 5EQD) because the opened KpUGM structure (PDB entry 2BI7)[40] used as a search model did not yield a molecular replacement solution. During refinement, torsional non-crystallographic symmetry restraints were applied to improve the geometry of chain B. Several combinations of translation−libration−screw (TLS) groups suggested by the TLSMD server were initially examined.[45,46] The optimal refinement strategy with a lowest $R_{factor}$ and $R_{free}$ involves splitting chain B into four TLS groups (residues 2−62, 63−235, 236−316, and 317−386) with chain A as a single TLS group. Data collection and refinement statistics are listed in Table 1. The coordinates and structure factors of GSG-CdUGM have been deposited as PDB entry 5EQF.

## RESULTS

**Structure of CdUGM-$His_6$.** To obtain structures of CdUGM in various conformations to contrast with the triazolothiadiazine-bound structure, two new CdUGM fusion proteins were crystallized. The first, CdUGM-$His_6$, afforded tetragonal crystals with one molecule in the asymmetric unit, corresponding to one half of the UGM dimer. Each crystallographically equivalent monomer is in an open conformation (Figure 2A). In this structure, the space where the substrate normally binds is occupied by an unexpected ligand, citrate. As expected for an open conformation, the mobile lid is not helical. The conserved arginine (R176) that normally contacts the pyrophosphoryl group of the substrate does not interact with the citrate ion (Figure 2A). A comparison with the structure of the CdUGM−triazolothiadiazine complex (PDB entry 4XGK) gave an overall C$\alpha$ RMSD of 0.88 Å over 386 residues. Thus, the conformations of the citrate-bound CdUGM and the small-molecule-bound CdUGM are similar (Figure 2B).

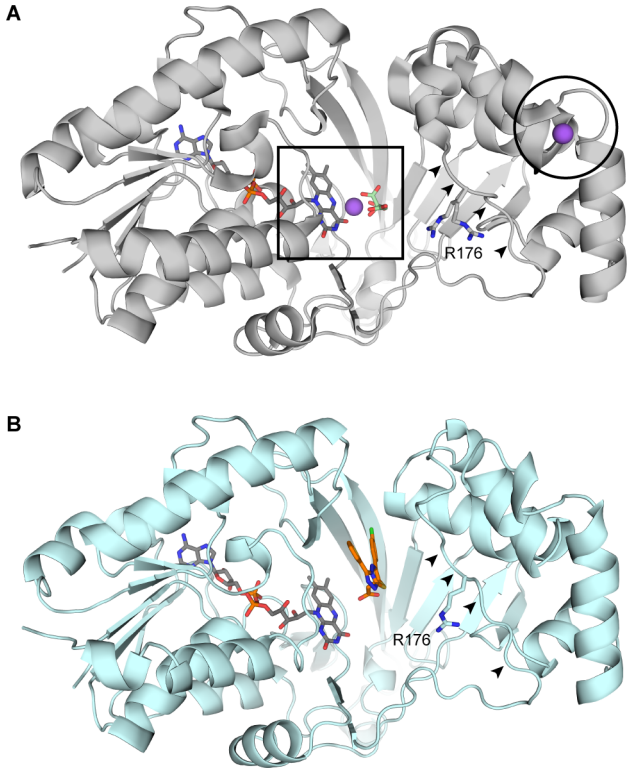


**Figure 2.** (A) Structure of CdUGM-$His_6$ in complex with sodium (purple) citrate (green). The enzyme is in an open conformation, as noted by the relationship between the mobile lid (arrows) and the oxidized FAD-containing active site (square). The circle indicates the position of a remote sodium ion binding site. (B) Structure of the CdUGM−triazolothiadiazine complex (PDB entry 4XGK). The open conformation of the mobile lid is indicated with arrows.

The citrate ion was identified on the basis of its shape and bonding partners and is located in the active site cavity adjacent to the FAD cofactor (Figure 3A). Citrate, which was present in the crystallization buffer, is anionic like the UDP-Gal*p* substrate. We analyzed the structure to evaluate features of the active site that may be exploited for future inhibitor design. The citrate ion forms salt bridges with UGM residues R288 and H290 and numerous ordered water molecules, thereby participating in a hydrogen-bonding network with the active site residues. A strong density feature was observed bridging the citrate ion and the oxidized FAD (Figure 3B). The absence of peaks in the $mF_o - DF_c$ map suggested the possibility that this density was the oxygen atom of a water molecule; however, irregular octahedral coordination geometry, bond lengths of approximately 2.4 Å[47] (Figure 3A), and proximity to the negatively charged citrate ion suggest that the peak corresponds to a sodium ion. An additional distal sodium ion binding site was also identified (Figure 2A and Figure S1). A potassium citrate buffer yielded no crystals, suggesting that the sodium ions were important for crystallization. When crystals grown with sodium citrate were soaked in potassium citrate buffer, a



DOI: 10.1021/acs.biochem.7b00189
*Biochemistry* 2017, 56, 3983−3992

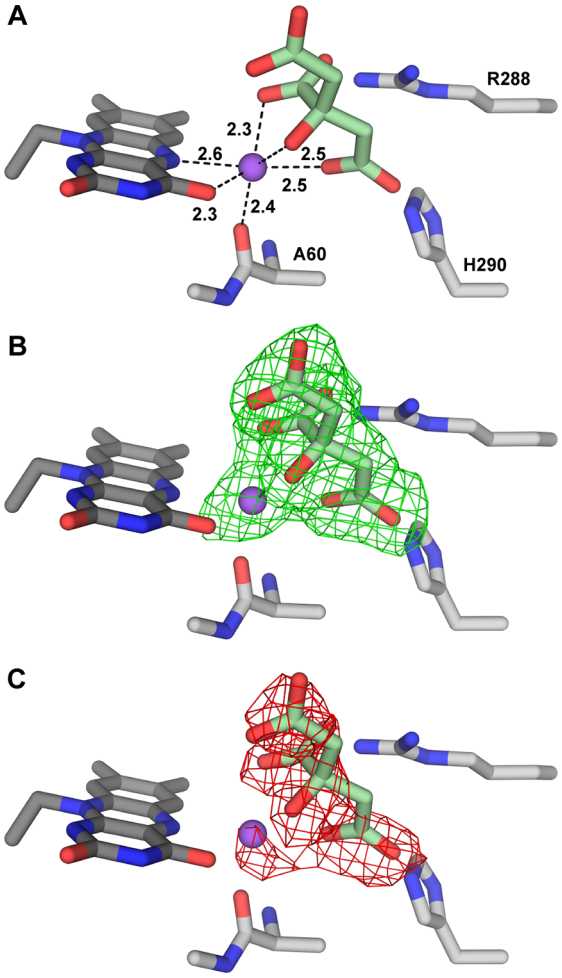


**Figure 3.** Depictions of the active site of the complex of CdUGM-$His_6$ with citrate (A) The sodium ion (purple) is complexed to the flavin (dark gray) and citrate (green). (B) The green mesh corresponds to the $mF_o - DF_c$ map contoured at $3\sigma$ after the citrate ion was removed and the structure refined with simulated annealing. (C) Structure factor amplitudes collected from a crystal soaked in potassium citrate-containing buffer lead to decreases in electron density. The red mesh corresponds to an $mF_o - DF_c$ difference Fourier map contoured at $-3\sigma$.

loss of electron density was observed for the active site sodium and citrate ions, as judged by the difference Fourier map (Figure 3C). These data suggest that it is a sodium ion coordinated to FAD, citrate ion, and the backbone carbonyl of A60. The likely presence of a cation near the flavin cofactor is intriguing, as the transition state for catalysis may involve flavin capture of an oxocarbenium ion.[1,48]

**GSG-CdUGM Bound to UDP.** A second CdUGM variant, GSG-CdUGM, was generated from cleavage of an N-terminal fusion protein. The wild-type enzyme bearing an N-terminal glycine-serine-glycine sequence crystallized in its dimeric state in the presence of UDP-Gal*p* (Figure 4). The electron density of chain A is well-defined. Chain B has elevated *B* factors and several weak side chain densities, although the backbone density could be unambiguously traced. Both monomers are in a closed conformation with the lid residues adopting helical structures. During the course of crystallization, UDP-Gal*p* was apparently converted to UDP. We considered the possibility that Gal*p* was disordered; however, the *B* factor for the $\beta$-phosphate is not elevated relative to that of the $\alpha$-phosphate,

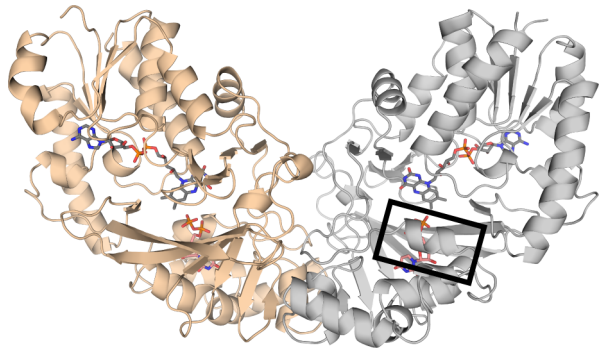

**Figure 4.** Structure of dimeric GSG-CdUGM. The closed lids form short helices covering the active sites (chain A colored gray, lid boxed, and chain B colored wheat, lid obscured).

and the electron density difference maps around UDP revealed no evidence of the presence of galactose. The observed hydrolysis is consistent with the mechanistic proposal that UDP functions as a leaving group in the interconversion of UDP-Gal*p* and UDP-Gal*f*.[1]

We previously found differences in the conformations of oxidized and reduced KpUGM−substrate complexes, raising the possibility that reduction of FAD triggers movement of the lid over the active site occupied by UDP-Gal*p*.[28] However, in the oxidized GSG-CdUGM structure, both monomers adopt a closed conformation. Each active site contains UDP, a putative intermediate in the catalytic mechanism. When the GSG-CdUGM structure is superimposed with the catalytically active, reduced, closed KpUGM,[28] the positions of active site residues are conserved (Figure 5). Underneath the closed helical lids, UDP fits snugly in the active site of GSG-CdUGM (Figure 5A) with the uracil ring stacking onto the $\pi$ face of Y157. Residues I174 and L177, along with F98 and I154, generate a hydrophobic box around the uracil moiety. The N3H group of uracil forms a hydrogen bond with the backbone carbonyl of F153, and O8 is recognized by the amide side chains of N278 and N280. The hydroxyl group of T158 forms hydrogen bonds with both O7 of uracil and the 2-hydroxyl group of ribose. The indole NH group of W162 engages in hydrogen bonding with the 3′-hydroxyl group of ribose. The pyrophosphoryl group is recognized by the side chains of R176 (from the lid), Y187, R288, Y326, and Y364. Upon superposition of UDP-Gal*p*-bound closed KpUGM on the structure of GSG-CdUGM, the UDP-Gal*p* substrate from the KpUGM structure fits well into the pocket of closed GSG-CdUGM (Figure 5B). Moreover, the superimposed anomeric carbon of Gal*p* is oriented as expected for catalysis: it is 3.4 Å from the nucleophilic nitrogen of FAD, which is comparable to the 3.6 Å difference observed in KpUGM. Thus, we conclude that GSG-CdUGM adopts a conformation similar to that of other catalytically active UGMs.

## DISCUSSION

Despite the availability of dozens of UGM structures, the only structure determined with a nonsubstrate analogue bound is that of CdUGM.[15] Here, our crystallization of CdUGM with unique termini resulted in two new crystal forms that provide information about the relationship between UGM conformation and ligand binding. The structure of CdUGM-$His_6$ identifies an unexpected citrate−$Na^+$−FAD complex, which binds to the open form of CdUGM. In the structure of CdUGM bound to triazolothiadiazine inhibitor **2**,[15] the enzyme



DOI: 10.1021/acs.biochem.7b00189
*Biochemistry* 2017, 56, 3983−3992

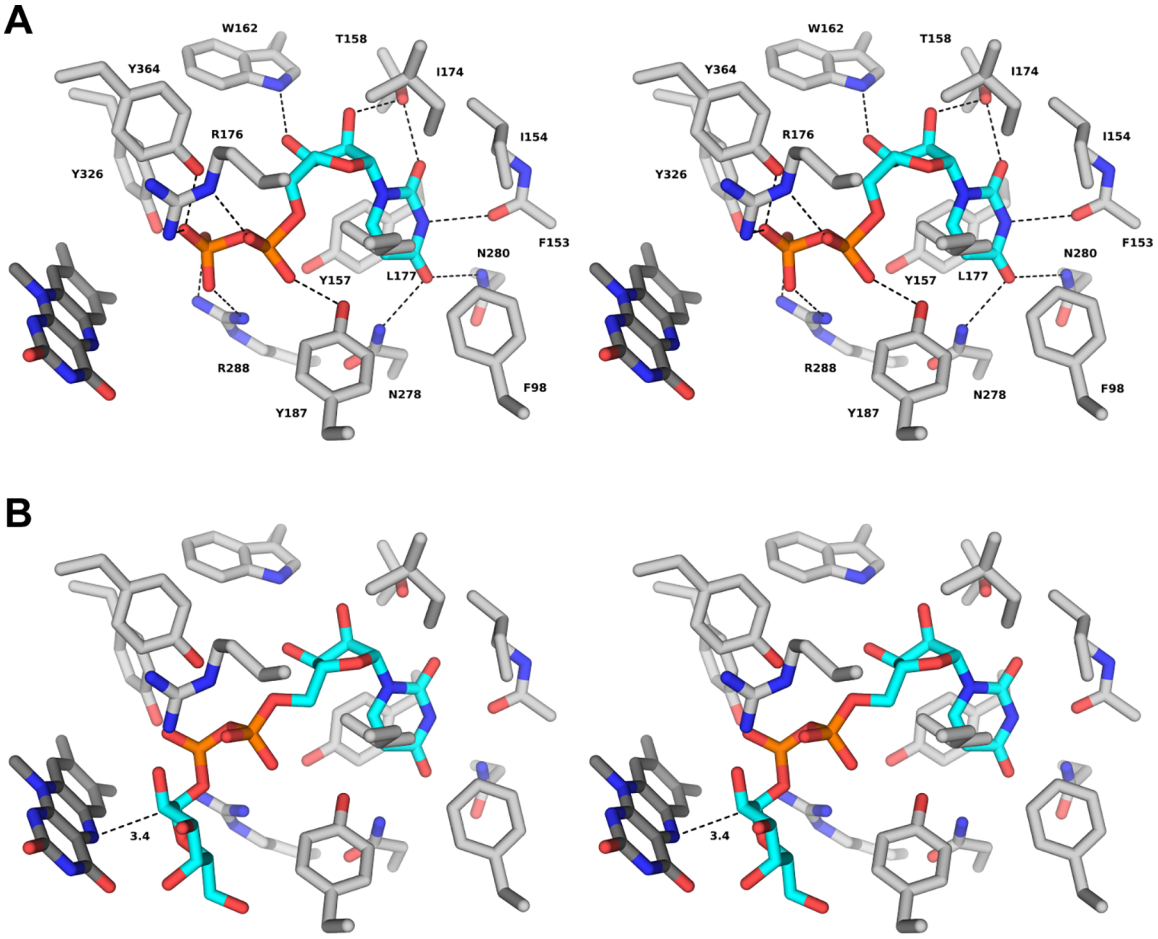


**Figure 5.** Comparison of the conformations of oxidized GSG-CdUGM bound to UDP and reduced KpUGM bound to UDP-Gal*p*. (A) Stereoview of the active site of GSG-CdUGM (chain A, gray) with bound UDP (cyan). All bond distances shown are ≤3.1 Å. (B) The oxidized UGM−UDP complex adopts a closed conformation similar to the catalytic conformation. Stereoview of the position of UDP-Gal*p* (cyan) from a structure of catalytically active KpUGM (PDB entry 3INT) superimposed on GSG-CdUGM (gray) with bound UDP (not shown).

also adopts an open conformation, but the presence of residual density hinted that the inhibitor might also bind the lid-closed conformation of CdUGM.[15] The conformation of the UGM complex reported herein is similar to that previously found for the enzyme bound to the triazolothiadiazine inhibitor.[15] Thus, the available data support the relevance of the open form of the complex. At the pH of the crystallization buffer, citrate exists predominantly as a dianion; therefore, it is of note that the mobile lid does not descend to allow the conserved arginine to neutralize the charge. Similarly, with carboxylate **2**, the mobile lid remains open. Interaction of the mobile loop arginine with the pyrophosphate moiety may be more favorable, thereby favoring lid closure upon substrate binding.

The structure of the CdUGM-His$_6$−sodium citrate complex features an active site pocket that could be targeted by small molecules. We therefore estimated the citrate dissociation constant. At a citrate concentration of 100 mM, the citrate was not at full occupancy in the crystallized complex. The dissociation constant ($K_d$) can be estimated using a simple equilibrium model and expressing [protein] and [protein:ligand] in occupancy terms ($K_d$ = [CdUGM-His$_6$][citrate]/[CdUGM-His$_6$−citrate] = 0.08 × 100 mM/0.92 = 8.7 mM), which provides a value in the range of 10 mM. This estimated $K_d$ is in the range relevant for molecular fragments that can result in useful ligands. This value is also the order of the intracellular citrate concentration in *Escherichia coli* (ranging from 2 to 20 mM depending on the growth medium).[49] Cellular citrate therefore has the potential to influence UGM conformation and regulate the enzyme's activity.

The citrate-bound structure could facilitate the design of novel inhibitors because citrate can serve as a steric and electronic probe of protein−small molecule interactions.[50] In the context of the CdUGM complex, either the triazolothiadiazine inhibitor or the citrate ion can form a salt bridge to the guanidinium group of R288 (Figure 6), but each occupies a slightly different region of the active site. Specifically, the small citrate ion binds deeper into the active site than does the larger inhibitor, suggesting triazolothiadiazine analogues that extend into the citrate binding site could bind more tightly. Indeed, this possibility is supported by the increased efficacy of small-molecule inhibitors in which the carboxylate is replaced by a larger *N*-acylsulfonamide group.[16]

The binding site identified in the CdUGM citrate complex differs from that occupied by an allosteric inhibitor identified recently. Specifically, a small-molecule heterocycle (MS-208) that differs in structure from the inhibitors described herein was reported to inhibit MtUGM ($K_i$ ∼ 400 $\mu$M).[32] The kinetics of inhibition together with computational and mutagenesis studies suggested that MS-208 does not compete directly with the substrate UDP-Gal*p* but rather binds in an allosteric site. The presence of multiple subsites highlights the flexibility of UGM.


DOI: 10.1021/acs.biochem.7b00189
*Biochemistry* 2017, 56, 3983−3992

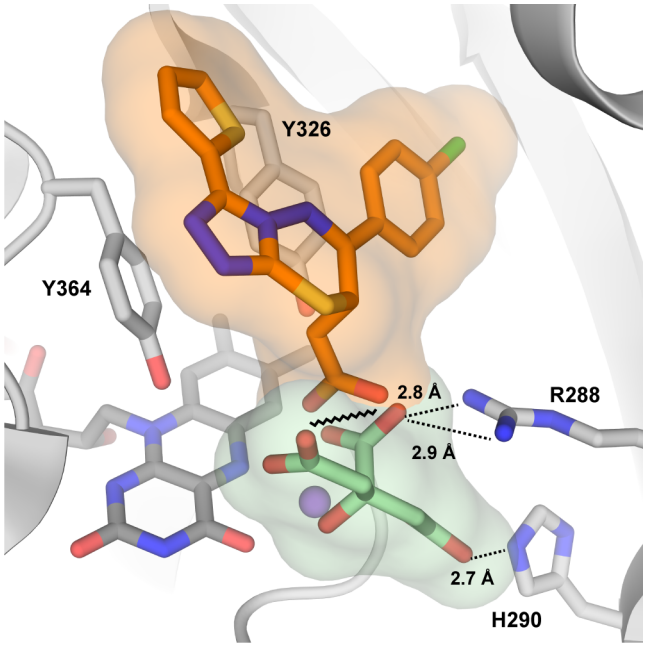


**Figure 6.** Structure of the triazolothiadiazine inhibitor (orange) from a previously reported cocrystal structure with CdUGM (PDB entry 4XGK) superimposed onto the structure of CdUGM-$His_6$ (gray) in complex with sodium citrate (purple and green, respectively). The clash between the carboxylates from the inhibitor and citrate is indicated with a zigzag line.

The molecular basis of our observation that triazolothiadiazine inhibitors **2** and **3**, as well as our other nonsubstrate inhibitors, are more effective against KpUGM than other orthologs is unclear. We considered the possibility that different inhibitors might bind open and/or closed forms and that the protein conformational equilibrium could influence inhibitor potency. With the GSG-CdUGM structure obtained herein, we were poised to compare the closed form of CdUGM with that of KpUGM. To this end, we superimposed the closed structure of KpUGM containing the predicted lowest-energy orientation of an inhibitor[15] onto the closed GSG-CdUGM structure. As predicted from conservation of the active site, no obvious clashes were detected with CdUGM (Figure 7A).[15]

The orientation of the triazolothiadizine inhibitor **2** inhibitor in the CdUGM complex[15] was not predicted by computational docking to be the most favorable (of lowest energy) (Figure 7A). To examine how this inhibitor orientation might impact binding, we superimposed the crystallographically determined inhibitor orientation on the closed CSG-CdUGM structure (Figure 7B). The inhibitor occupies a space that would clash with the position of lid residue R176 (Figure 7B). This conserved positively charged side chain[3,31] is present in all UGM orthologs and interacts with the substrate through hydrogen bonding to galactose hydroxyl groups and/or the pyrophosphoryl group.[26,28,30,33,51] This "dynamic arginine (R176)"[31] may adopt an alternate side chain rotamer to alleviate the steric clash with the triazolothiadiazine inhibitor (Figure 7B). Although the flexibility of R176 could differ between UGMs, our data suggest that it is flexible in both KpUGM and CdUGM. Specifically, in the closed KpUGM structure (PDB entry 3INT), the temperature factors of the closed lid and R176 were higher than those in the rest of the protein. Similarly in CSG-CdUGM, two side chain rotamers for R176 were present in the open structure (Figure 2A). In contrast, distinct differences in the position of a different residue, Y364, were detected in closed conformations of CdUGM and KpUGM. In GSG-CdUGM, this residue was in the active site, such that the side chain phenol ring was twisted almost perpendicular to its orientation in the inhibitor-bound open structure (Figure 7B). In this way, Y364 may prevent the inhibitor from binding CdUGM in the closed conformation. A similar inward-oriented position of the Y364 equivalent was observed in the closed structure of MtUGM.[26] Notably, no such conformational change of the corresponding residue (Y349) was detected in KpUGM (Figure 7C).[28] We also noted that N173 in CdUGM (N177 in MtUGM) was replaced in KpUGM with an isoleucine that may favorably interact with the hydrophobic chlorophenyl ring of the inhibitor to increase affinity (Figure 7C). These data suggest that the orientation of the CdUGM complex determined by X-ray crystallography (PDB entry 4XGK), with the triazolothiadiazine inhibitor binding to the open form of CdUGM, reflects the mode of binding of the inhibitor to *C. diphtheriae* and *M. tuberculosis*. These results highlight the relevance of the CdUGM−inhibitor complex for advancing inhibitor design.

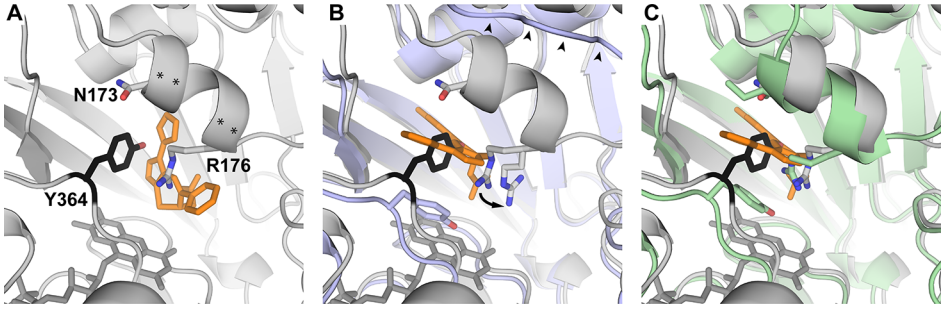


**Figure 7.** Comparison of known and docked small-molecule inhibitor complexes highlighting Y364 (black) movement. All superpositions were performed using protein $\alpha$-carbons with refinement to optimize the fit. Changes in the lid conformation between open and closed forms are denoted with asterisks (closed form, panel A) or a row of arrows (open form, panel B). (A) Computational model of the triazolothiadiazine inhibitor (orange) complex derived from the closed form of KpUGM (PDB entry 3INT) superimposed on the structure of the closed form of GSG-CdUGM (gray). (B) Orientation of the inhibitor (orange) in the crystalline CdUGM complex (light blue, PDB entry 4XGK), which is in the open form. Superimposed on this complex is the closed form of GSG-CdUGM (gray). A likely alternative rotamer for R176 is shown. The Y364 (black) that clashes with the inhibitor is highlighted. (C) Superposition of the closed GSG-CdUGM (gray) structure with the closed form of KpUGM (green) (PDB entry 3INT) with the crystallized pose of the triazolothiadiazine inhibitor (orange). CdUGM residue numbering is shown.



DOI: 10.1021/acs.biochem.7b00189
*Biochemistry* 2017, 56, 3983−3992

Often the most efficacious inhibitors are those that bind the closed form over the open form of an enzyme. For example, the inhibitor imatinib targets Abl kinase over other closely related kinases because imatinib interacts with the conformation of Abl in which the activation loop is closed.[52] In analogy, inhibitor **2** may bind the closed form of KpUGM but the open form of CdUGM, MtUGM, or other UGM orthologs. Though we cannot rule out binding to the open form of the KpUGM, we expect that the affinity of binding to the closed complex would higher than that of binding to the open state. All of the known X-ray structures of prokaryotic UGM orthologs (CdUGM, MtUGM, and DrUGM),[30] with the exception of KpUGM, indicate Y364 undergoes conformational change. This change is coupled to lid closing and would preclude binding of the inhibitor to the closed state.

The amino acid residue differences between prokaryotic and eukaryotic UGM active sites are large, and further study is needed to understand the molecular basis for differences in inhibitor binding between prokaryotic and eukaryotic enzymes.[31] For example, there are at least two mobile lids covering the active site in eukaryotic UGM, compared to one in prokaryotic UGMs,[31] which complicates the analysis of the basis for differences in inhibitor affinity. Still, the potencies of 2-aminothiazole small-molecule inhibitors against the *C. elegans* UGM are superior to those observed for CdUGM and MtUGM and similar to those observed against KpUGM.[11] Consistent with the prediction from the analysis presented here, the residue corresponding to Y364 in eukaryotic UGMs (AfUGM[33] and TcUGM[34]) is similar to that of KpUGM in that no dramatic change in position is observed in the closed conformation of the eukaryotic UGMs.

The role of UGM cofactor reduction is another key issue for the enzyme's conformation and therefore inhibition. Reduction of the FAD cofactor is required for UGM activity.[3] The isoalloxazine ring of oxidized FAD is planar but upon reduction adopts a puckered, butterfly conformation. In crystals of KpUGM in complex with the substrate UDP-Gal*p*, the flavin could be reduced within the same crystal form, a process that accompanied further closure of the lid.[28] Our structure of oxidized GSG-CdUGM in complex with UDP indicates the inactive enzyme can adopt a closed conformation analogous to that observed for the catalytically competent KpUGM. Other closed UGM orthologs have been crystallized with oxidized FAD either with or without bound substrates, including DrUGM,[30] EcUGM,[3] AfUGM,[51] and TcUGM.[34] These findings suggest that the energy barrier for conformational change is small, regardless of the FAD oxidation state. Thus, a low-barrier conformational change could be a universal attribute of UGMs, raising the possibility that inhibitors could target specific UGM conformational states. Inhibitor trapping of UGM in an inactive conformation could be an effective inhibition strategy.[32] Indeed, many kinase inhibitors bind to and stabilize an inactive conformation of their target enzymes.[53−56] Our data thus far suggest inhibitors that can occupy the closed, oxidized state of the enzyme might be especially effective. They would not only prevent substrate binding but also limit the access of reducing agents to the isoalloxazine ring, thereby preventing generation of the catalytically competent state.

Efforts to understand UGM structural dynamics are opening new possibilities for improving inhibitor potency. The dramatic variation in UGM lid conformations[31] suggests that inhibitors could be generated that specifically block particular UGM orthologs. Such inhibitors will be useful for targeting pathogens uniquely. Moreover, optimizing and identifying small molecules that can be accommodated in the closed, oxidized form of UGM should lead to next-generation inhibitors with enhanced efficacy.

## ■ ASSOCIATED CONTENT

### Supporting Information

The Supporting Information is available free of charge on the ACS Publications website at DOI: 10.1021/acs.biochem.7b00189.

Description of the remote sodium ion binding site and the corresponding figure (Figure S1) (PDF)

## ■ AUTHOR INFORMATION


### Corresponding Authors

*Telephone: 608-265-3566. E-mail: forest@bact.wisc.edu.

*Telephone: 608-262-0541. E-mail: kiessling@chem.wisc.edu.

### ORCID

Kittikhun Wangkanont: 0000-0002-7190-2955

Laura L. Kiessling: 0000-0001-6829-1500

### Present Address

‖K.W.: Department of Biochemistry, Faculty of Science, Chulalongkorn University, Bangkok, Thailand.


### Author Contributions

K.W., K.T.F., and L.L.K. designed the study and analyzed the results. K.W. and V.J.W. performed the experiments. K.W., K.T.F., and L.L.K. wrote the manuscript with input from V.J.W.


### Funding

This research was supported by National Institute of Allergy and Infectious Disease Grants R01 AI063596 and R01 AI126592 (to L.L.K.) and by National Science Foundation (NSF) Grant IOS1353674 (to K.T.F. and H. Goodrich-Blair). K.W. was supported by a fellowship from the Development and Promotion of Science and Technology Talents Project of Thailand. V.J.W. was supported by a NSF Graduate Research Fellowship (DGE-1256259).


### Notes

The authors declare no competing financial interest.

## ■ ACKNOWLEDGMENTS


These studies used resources of the Advanced Photon Source, a U.S. Department of Energy (DOE) Office of Science User Facility operated by Argonne National Laboratory under Contract DE-AC02-06CH11357. Use of LS-CAT Sector 21 was supported by the Michigan Economic Development Corp. and the Michigan Technology Tri-Corridor (Grant 085P1000817). Use of the Stanford Synchrotron Radiation Lightsource (SLAC National Accelerator Laboratory) is supported by the DOE Office of Science, Office of Basic Energy Sciences, under Contract DE-AC02-76SF00515. The SSRL Structural Molecular Biology Program is supported by the DOE Office of Biological and Environmental Research and by the National Institute of General Medical Sciences (NIGMS) (Grant P41GM103393). We thank Dr. Annie Héroux (Brookhaven National Laboratory, Upton, NY) for measuring preliminary X-ray diffraction data at beamline X25 of the National Synchrotron Light Source, which is supported principally by the DOE Offices of Biological and Environmental Research and Basic Energy Sciences, the National Center for Research Resources (P41RR012408), and the NIGMS




DOI: 10.1021/acs.biochem.7b00189
*Biochemistry* 2017, 56, 3983−3992

(P41GM103473). We thank Dr. Robert A. Brown and Virginia A. Kincaid for helpful comments during manuscript preparation.

## ■ ABBREVIATIONS

UGM, UDP-galactopyranose mutase; UDP, uridine 5′-diphosphate; Gal*f*, galactofuranose; Gal*p*, galactopyranose; EG 5000 MME, polyethylene glycol 5000 monomethyl ether; FAD, flavin adenine dinucleotide; RMSD, root-mean-square deviation.

## ■ REFERENCES

(1) Soltero-Higgin, M., Carlson, E. E., Gruber, T. D., and Kiessling, L. L. (2004) A unique catalytic mechanism for UDP-galactopyranose mutase. *Nat. Struct. Mol. Biol. 11*, 539−543.

(2) Nassau, P. M., Martin, S. L., Brown, R. E., Weston, A., Monsey, D., McNeil, M. R., and Duncan, K. (1996) Galactofuranose biosynthesis in Escherichia coli K-12: identification and cloning of UDP-galactopyranose mutase. *J. Bacteriol. 178*, 1047−1052.

(3) Sanders, D. A., Staines, A. G., McMahon, S. A., McNeil, M. R., Whitfield, C., and Naismith, J. H. (2001) UDP-galactopyranose mutase has a novel structure and mechanism. *Nat. Struct. Biol. 8*, 858−863.

(4) Gastebois, A., Clavaud, C., Aimanianda, V., and Latge, J. P. (2009) Aspergillus fumigatus: cell wall polysaccharides, their biosynthesis and organization. *Future Microbiol. 4*, 583−595.

(5) Sassetti, C. M., Boyd, D. H., and Rubin, E. J. (2003) Genes required for mycobacterial growth defined by high density mutagenesis. *Mol. Microbiol. 48*, 77−84.

(6) Pan, F., Jackson, M., Ma, Y., and McNeil, M. (2001) Cell wall core galactofuran synthesis is essential for growth of mycobacteria. *J. Bacteriol. 183*, 3991−3998.

(7) Suzuki, E., Tanaka, A. K., Toledo, M. S., Takahashi, H. K., and Straus, A. H. (2002) Role of beta-D-galactofuranose in Leishmania major macrophage invasion. *Infect. Immun. 70*, 6592−6596.

(8) Tefsen, B., Ram, A. F., van Die, I., and Routier, F. H. (2012) Galactofuranose in eukaryotes: aspects of biosynthesis and functional impact. *Glycobiology 22*, 456−469.

(9) Novelli, J. F., Chaudhary, K., Canovas, J., Benner, J. S., Madinger, C. L., Kelly, P., Hodgkin, J., and Carlow, C. K. (2009) Characterization of the Caenorhabditis elegans UDP-galactopyranose mutase homolog glf-1 reveals an essential role for galactofuranose metabolism in nematode surface coat synthesis. *Dev. Biol. 335*, 340−355.

(10) Beverley, S. M., Owens, K. L., Showalter, M., Griffith, C. L., Doering, T. L., Jones, V. C., and McNeil, M. R. (2005) Eukaryotic UDP-galactopyranose mutase (GLF gene) in microbial and metazoal pathogens. *Eukaryotic Cell 4*, 1147−1154.

(11) Wesener, D. A., May, J. F., Huffman, E. M., and Kiessling, L. L. (2013) UDP-galactopyranose mutase in nematodes. *Biochemistry 52*, 4391−4398.

(12) Richards, M. R., and Lowary, T. L. (2009) Chemistry and biology of galactofuranose-containing polysaccharides. *ChemBioChem 10*, 1920−1938.

(13) Schmalhorst, P. S., Krappmann, S., Vervecken, W., Rohde, M., Muller, M., Braus, G. H., Contreras, R., Braun, A., Bakker, H., and Routier, F. H. (2008) Contribution of galactofuranose to the virulence of the opportunistic pathogen Aspergillus fumigatus. *Eukaryotic Cell 7*, 1268−1277.

(14) Dykhuizen, E. C., May, J. F., Tongpenyai, A., and Kiessling, L. L. (2008) Inhibitors of UDP-galactopyranose mutase thwart mycobacterial growth. *J. Am. Chem. Soc. 130*, 6706−6707.

(15) Kincaid, V. A., London, N., Wangkanont, K., Wesener, D. A., Marcus, S. A., Heroux, A., Nedyalkova, L., Talaat, A. M., Forest, K. T., Shoichet, B. K., and Kiessling, L. L. (2015) Virtual Screening for UDP-Galactopyranose Mutase Ligands Identifies a New Class of Antimycobacterial Agents. *ACS Chem. Biol. 10*, 2209−2218.

(16) Winton, V. J., Aldrich, C., and Kiessling, L. L. (2016) Carboxylate Surrogates Enhance the Antimycobacterial Activity of UDP-Galactopyranose Mutase Probes. *ACS Infect. Dis. 2*, 538−543.

(17) Wesener, D. A., Levengood, M. R., and Kiessling, L. L. (2017) Comparing galactan biosynthesis in Mycobacterium tuberculosis and Corynebacterium diphtheriae. *J. Biol. Chem. 292*, 2944−2955.

(18) Barraud, O., Badell, E., Denis, F., Guiso, N., and Ploy, M. C. (2011) Antimicrobial drug resistance in Corynebacterium diphtheriae mitis. *Emerging Infect. Dis. 17*, 2078−2080.

(19) Ansiaux, C., N'Go, I., and Vincent, S. P. (2012) Reversible and efficient inhibition of UDP-galactopyranose mutase by electrophilic, constrained and unsaturated UDP-galactitol analogues. *Chem. - Eur. J. 18*, 14860−14866.

(20) Caravano, A., Dohi, H., Sinay, P., and Vincent, S. P. (2006) A new methodology for the synthesis of fluorinated exo-glycals and their time-dependent inhibition of UDP-galactopyranose mutase. *Chem. - Eur. J. 12*, 3114−3123.

(21) El Bkassiny, S., N'Go, I., Sevrain, C. M., Tikad, A., and Vincent, S. P. (2014) Synthesis of a novel UDP-carbasugar as UDP-galactopyranose mutase inhibitor. *Org. Lett. 16*, 2462−2465.

(22) Itoh, K., Huang, Z., and Liu, H. W. (2007) Synthesis and analysis of substrate analogues for UDP-galactopyranose mutase: implication for an oxocarbenium ion intermediate in the catalytic mechanism. *Org. Lett. 9*, 879−882.

(23) Kuppala, R., Borrelli, S., Slowski, K., Sanders, D. A., Ravindranathan Kartha, K. P., and Pinto, B. M. (2015) Synthesis and biological evaluation of nonionic substrate mimics of UDP-Galp as candidate inhibitors of UDP galactopyranose mutase (UGM). *Bioorg. Med. Chem. Lett. 25*, 1995−1997.

(24) Liautard, V., Desvergnes, V., Itoh, K., Liu, H. W., and Martin, O. R. (2008) Convergent and stereoselective synthesis of iminosugar-containing Galf and UDP-Galf mimicks: evaluation as inhibitors of UDP-Gal mutase. *J. Org. Chem. 73*, 3103−3115.

(25) Partha, S. K., Sadeghi-Khomami, A., Slowski, K., Kotake, T., Thomas, N. R., Jakeman, D. L., and Sanders, D. A. (2010) Chemoenzymatic synthesis, inhibition studies, and X-ray crystallographic analysis of the phosphono analog of UDP-Galp as an inhibitor and mechanistic probe for UDP-galactopyranose mutase. *J. Mol. Biol. 403*, 578−590.

(26) van Straaten, K. E., Kuttiyatveetil, J. R., Sevrain, C. M., Villaume, S. A., Jimenez-Barbero, J., Linclau, B., Vincent, S. P., and Sanders, D. A. (2015) Structural basis of ligand binding to UDP-galactopyranose mutase from Mycobacterium tuberculosis using substrate and tetrafluorinated substrate analogues. *J. Am. Chem. Soc. 137*, 1230−1244.

(27) Borrelli, S., Zandberg, W. F., Mohan, S., Ko, M., Martinez-Gutierrez, F., Partha, S. K., Sanders, D. A., Av-Gay, Y., and Pinto, B. M. (2010) Antimycobacterial activity of UDP-galactopyranose mutase inhibitors. *Int. J. Antimicrob. Agents 36*, 364−368.

(28) Gruber, T. D., Westler, W. M., Kiessling, L. L., and Forest, K. T. (2009) X-ray crystallography reveals a reduced substrate complex of UDP-galactopyranose mutase poised for covalent catalysis by flavin. *Biochemistry 48*, 9171−9173.

(29) Ponnusamy, R., Lebedev, A. A., Pahlow, S., and Lohkamp, B. (2014) Crystal structure of human CRMP-4: correction of intensities for lattice-translocation disorder. *Acta Crystallogr., Sect. D: Biol. Crystallogr. 70*, 1680−1694.

(30) Karunan Partha, S., van Straaten, K. E., and Sanders, D. A. (2009) Structural basis of substrate binding to UDP-galactopyranose mutase: crystal structures in the reduced and oxidized state complexed with UDP-galactopyranose and UDP. *J. Mol. Biol. 394*, 864−877.

(31) Tanner, J. J., Boechi, L., Andrew McCammon, J., and Sobrado, P. (2014) Structure, mechanism, and dynamics of UDP-galactopyranose mutase. *Arch. Biochem. Biophys. 544*, 128−141.

(32) Shi, Y., Colombo, C., Kuttiyatveetil, J. R., Zalatar, N., van Straaten, K. E., Mohan, S., Sanders, D. A., and Pinto, B. M. (2016) A second, druggable binding site in UDP-galactopyranose mutase from Mycobacterium tuberculosis? *ChemBioChem 17*, 2264−2273.



DOI: 10.1021/acs.biochem.7b00189
*Biochemistry* 2017, 56, 3983−3992

(33) Dhatwalia, R., Singh, H., Oppenheimer, M., Karr, D. B., Nix, J. C., Sobrado, P., and Tanner, J. J. (2012) Crystal structures and small-angle x-ray scattering analysis of UDP-galactopyranose mutase from the pathogenic fungus Aspergillus fumigatus. *J. Biol. Chem. 287*, 9041−9051.
(34) Dhatwalia, R., Singh, H., Oppenheimer, M., Sobrado, P., and Tanner, J. J. (2012) Crystal structures of Trypanosoma cruzi UDP-galactopyranose mutase implicate flexibility of the histidine loop in enzyme activation. *Biochemistry 51*, 4968−4979.
(35) Carugo, O. (2011) Participation of protein sequence termini in crystal contacts. *Protein Sci. 20*, 2121−2124.
(36) Fullerton, S. W., Daff, S., Sanders, D. A., Ingledew, W. J., Whitfield, C., Chapman, S. K., and Naismith, J. H. (2003) Potentiometric analysis of UDP-galactopyranose mutase: stabilization of the flavosemiquinone by substrate. *Biochemistry 42*, 2104−2109.
(37) Soltero-Higgin, M., Carlson, E. E., Phillips, J. H., and Kiessling, L. L. (2004) Identification of inhibitors for UDP-galactopyranose mutase. *J. Am. Chem. Soc. 126*, 10532−10533.
(38) Otwinowski, Z., and Minor, W. (1997) Processing of X-ray diffraction data collected in oscillation mode. In *Methods in Enzymology: Macromolecular Crystallography, Part A* (Carter, C. W., Jr., and Sweet, R. M., Eds.) pp 307−326, Academic Press, New York.
(39) McCoy, A. J., Grosse-Kunstleve, R. W., Adams, P. D., Winn, M. D., Storoni, L. C., and Read, R. J. (2007) Phaser crystallographic software. *J. Appl. Crystallogr. 40*, 658−674.
(40) Beis, K., Srikannathasan, V., Liu, H., Fullerton, S. W., Bamford, V. A., Sanders, D. A., Whitfield, C., McNeil, M. R., and Naismith, J. H. (2005) Crystal structures of Mycobacteria tuberculosis and Klebsiella pneumoniae UDP-galactopyranose mutase in the oxidised state and Klebsiella pneumoniae UDP-galactopyranose mutase in the (active) reduced state. *J. Mol. Biol. 348*, 971−982.
(41) Moriarty, N., Grosse-Kunstleve, R., and Adams, P. (2009) electronic Ligand Builder and Optimization Workbench (eLBOW): a tool for ligand coordinate and restraint generation. *Acta Crystallogr., Sect. D: Biol. Crystallogr. 65*, 1074−1080.
(42) Emsley, P., Lohkamp, B., Scott, W. G., and Cowtan, K. (2010) Features and development of Coot. *Acta Crystallogr., Sect. D: Biol. Crystallogr. 66*, 486−501.
(43) Afonine, P. V., Grosse-Kunstleve, R. W., and Adams, P. D. (2005) The Phenix refinement framework. *Collaborative Computational Project 4 Newsletter 42*, 8.
(44) Chen, V. B., III, Arendall, W. B., Headd, J. J., Keedy, D. A., Immormino, R. M., Kapral, G. J., Murray, L. W., Richardson, J. S., and Richardson, D. C. (2010) MolProbity: all-atom structure validation for macromolecular crystallography. *Acta Crystallogr., Sect. D: Biol. Crystallogr. 66*, 12−21.
(45) Painter, J., and Merritt, E. A. (2006) Optimal description of a protein structure in terms of multiple groups undergoing TLS motion. *Acta Crystallogr., Sect. D: Biol. Crystallogr. 62*, 439−450.
(46) Painter, J., and Merritt, E. A. (2006) TLSMD web server for the generation of multi-group TLS models. *J. Appl. Crystallogr. 39*, 109−111.
(47) Harding, M. M. (2002) Metal-ligand geometry relevant to proteins and in proteins: sodium and potassium. *Acta Crystallogr., Sect. D: Biol. Crystallogr. 58*, 872−874.
(48) Mehra-Chaudhary, R., Dai, Y., Sobrado, P., and Tanner, J. J. (2016) In Crystallo Capture of a Covalent Intermediate in the UDP-Galactopyranose Mutase Reaction. *Biochemistry 55*, 833−836.
(49) Bennett, B. D., Kimball, E. H., Gao, M., Osterhout, R., Van Dien, S. J., and Rabinowitz, J. D. (2009) Absolute metabolite concentrations and implied enzyme active site occupancy in Escherichia coli. *Nat. Chem. Biol. 5*, 593−599.
(50) Brenk, R., Irwin, J. J., and Shoichet, B. K. (2005) Here be dragons: docking and screening in an uncharted region of chemical space. *J. Biomol. Screening 10*, 667−674.
(51) van Straaten, K. E., Routier, F. H., and Sanders, D. A. (2012) Structural insight into the unique substrate binding mechanism and flavin redox state of UDP-galactopyranose mutase from Aspergillus fumigatus. *J. Biol. Chem. 287*, 10780−10790.
(52) Cowan-Jacob, S. W., Fendrich, G., Floersheimer, A., Furet, P., Liebetanz, J., Rummel, G., Rheinberger, P., Centeleghe, M., Fabbro, D., and Manley, P. W. (2007) Structural biology contributions to the discovery of drugs to treat chronic myelogenous leukaemia. *Acta Crystallogr., Sect. D: Biol. Crystallogr. 63*, 80−93.
(53) Garuti, L., Roberti, M., and Bottegoni, G. (2010) Non-ATP competitive protein kinase inhibitors. *Curr. Med. Chem. 17*, 2804−2821.
(54) Ung, P. M., and Schlessinger, A. (2015) DFGmodel: predicting protein kinase structures in inactive states for structure-based discovery of type-II inhibitors. *ACS Chem. Biol. 10*, 269−278.
(55) Eathiraj, S., Palma, R., Hirschi, M., Volckova, E., Nakuci, E., Castro, J., Chen, C. R., Chan, T. C., France, D. S., and Ashwell, M. A. (2011) A novel mode of protein kinase inhibition exploiting hydrophobic motifs of autoinhibited kinases: discovery of ATP-independent inhibitors of fibroblast growth factor receptor. *J. Biol. Chem. 286*, 20677−20687.
(56) Liu, Y., and Gray, N. S. (2006) Rational design of inhibitors that bind to inactive kinase conformations. *Nat. Chem. Biol. 2*, 358−364.


DOI: 10.1021/acs.biochem.7b00189
*Biochemistry* 2017, 56, 3983−3992